Design of sliding mode observer for the estimation of train car positions and in-train forces

Fawzia Bouchama, Michael Defoort, Denis Berdjag, Jimmy Lauber

Available online at www.sciencedirect.com

ScienceDirect

IFAC PapersOnLine 54-4 (2021) 98–105

Design of sliding mode observer for the estimation of train car positions and in-train forces

Hiba Fawzia Bouchama * **Michael Defoort** ** **Denis Berdjag** *** **Jimmy Lauber** **

* *Technological research institute (IRT) of the railway sector RAILENIUM (e-mail:hiba.bouchama@railenium.eu)*
** *Univ. Polytechnique Hauts-de-France, LAMIH, CNRS, UMR 8201, F-59313 Valenciennes, France*
INSA Hauts-de-France, F-59313 Valenciennes, France (e-mail: michael.defoort; jimmy.lauber@uphf.fr)
*** *Univ. Polytechnique Hauts-de-France, LAMIH, CNRS, UMR 8201, F-59313 Valenciennes, France (e-mail:denis.berdjag@uphf.fr)*

Abstract:
For the control design of freight trains, the estimation of in-train forces is crucial to avoid safety issues caused by the possible failure of car couplers under excessive stress. However, the in-train forces and the relative positions of adjacent train cars are not directly measurable. To address this issue, this paper designs estimators of train car positions and in-train forces using only locomotive-based measurements. Using the multi-point train model, a cascade structure of robust sliding mode differentiators is developed. It provides finite-time estimation of train car positions and in-train forces. Simulation results illustrate the feasibility of the proposed approach.

Keywords: Autonomous train, In-train forces, Sliding mode observer, Robust differentiator.

1. INTRODUCTION

Train Control Systems (TCS) aim to drive autonomous or semi-autonomous trains safely and efficiently. To reach this objective, TCS require reliable data and accurate system modeling. Different approaches can be applied depending on the amount of available information and the desired objectives. The modeling of the train dynamics is challenging. Indeed, the kinematics is described by three translational motions (longitudinal, lateral and vertical) and three rotational motions (yaw, pitch and roll), resulting in a six degrees of freedom model (Wang and Xia, 2003). However, for the guided transport systems, the longitudinal motion is dominant and the control model complexity can be significantly reduced. The single-point train model, for which the model is reduced to a single-point mass object, is the most commonly used model in solving train operation problems (Uyulan and Gokasan, 2018; Chen et al., 2014, 2016; Wang and Jia, 2018), for short trains such as passenger trains. However, this model is not sufficiently accurate when there is a large number of cars attached by flexible couplers. To jointly consider the motion of the locomotive, the motion of the train cars and the relevant in-train forces between adjacent train cars, the so-called multi-point train model is considered. In such model, vehicles are reduced to point mass connected by coupler devices (Xia and Zhang, 2011; Chou et al., 2007; Gao et al., 2013; Zhu and Xia, 2015). This model is sufficient to represent the accordion-like effect of long freight trains.

One of the challenges in the design of TCS is to avoid an excessive stress on the couplings, which may lead to coupler breaking due to traction, i.e. loss of wagons, or derailment due to compression (Liu et al., 2017b). The stress on couplers is modeled by in-train forces, and the TCS strategy is to keep these forces within acceptable limits. For instance, the in-train force limits appear in the emergency braking condition. This problem has been investigated in several works (Pei-Xin, 1994; Yang et al., 2014; Gao et al., 2017). Furthermore, a number of control strategies have been developed in the literature to deal with the speed tracking problem for the train, while ensuring some performances in terms of in-train force, energy consumption and traveling time (Xia and Zhang, 2011). In (Chou and Xia, 2007), a linear quadratic regulator (LQR) was proposed by considering the minimum in-train force and energy consumption. An active vibration control of multi-body system based on active damping was investigated to reduce the in-train forces (Tang et al., 2006). (Zhang and Zhuan, 2014) proposed a model predictive control method to optimize the controller under two penalty functions: one for the braking forces and the other one for the coupler elastic effects.

The above-mentioned works are based on the assumption that the displacement of each car can be obtained

10.1016/j.ifacol.2021.10.017

precisely. Furthermore, trains run under different operational conditions, making the estimation problem more complex. In (Liu et al., 2017a), a multi-point train model is constructed to obtain a multi-agent system, and a distributed cooperative observer is proposed to estimate the relative displacement of adjacent vehicles. However, such an approach requires at least one measurement for each agent (vehicle). Unfortunately, in practice, the train cars are not equipped with sensors and data transmission network which transmit information to the TCS. Hence, a realistic design of estimators for the in-train forces and train car positions must rely on the available sensors on the locomotive.

In real-world situations, the train dynamics is also affected by disturbances, parametric variations and possible device faults. The wheel-rail adhesion between the wheel and the track is one of these disturbances. Indeed, it directly impacts the transmission of the traction/braking torque and can be interpreted as a variable actuator saturation which causes wheel skidding. Multiple models and approximations of the adhesion force are proposed in the literature for cars and trains (see Kalker (1979); Burckhardt (1993); Pacejka (2002)). Nevertheless, in railways, designing a model that is both sufficiently accurate and cost effective for control applications remains an open issue.

In the literature, different approaches have been proposed to design estimators. The first approach is based on the design of observers, which use the available sensor measurements and the analytical model of the system to reconstruct unmeasured states (Chen, 2004; Lien, 2004; Kommuri et al., 2016; Aguiar et al., 2018; Losero et al., 2015). The second one is based on the design of robust differentiators to reconstruct the signal derivatives while filtering measurement noises such as high-gain observers (Dabroom and Khalil, 1999), or sliding mode observers (Cruz-Zavala et al., 2011).

In this paper, based on the works of (Levant, 2003; Levant and Livne, 2020a), we design a cascade of sliding mode differentiators for the considered system. An approach to estimate the in-train forces and train car positions under variable wheel-rail adhesion, using locomotive position and its wheel angular speed is presented. The cascade structure of n observers is used to estimate the wheel-rail adhesion force, and the in-train forces and train car positions. The proposed sliding mode approach ensures finite-time convergence of the estimation error.

The paper is organized as follows. Section 2 presents some preliminaries on Train Control Systems and presents the problem statement. Section 3 introduces the main contribution: the cascade observation scheme based on sliding mode differentiators. Simulation results are provided in Section 4, and finally, Section 5 brings conclusions and future works.

2. PROBLEM FORMULATION

2.1 Preliminaries on Train Control Systems

Automatic Train Control (ATC) system consists of the Automatic Train Protection (ATP), Automatic Train supervision (ATS) and Automatic Train Operation (ATO) systems. The ATO system deals with almost all the control issues of the train operation, and thus performs a crucial role for the train. The primary task of the ATO system is to control the train speed in real-time based on the desired speed profile (see Figure 1). An effective algorithm must not only accurately track the desired position and velocity, but also achieve other performances, such as energy saving, comfort, and so on.

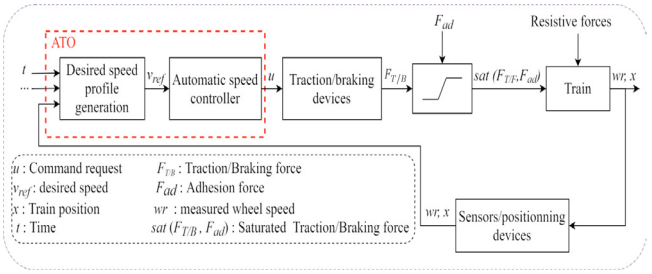

Fig. 1. Overview of the train speed control by the ATO system.

The automatic train operation is a highly complex process which involves acceleration, cruising, coasting and braking (see Figure 2), while taking into account several parametric variations and external disturbances, due to for instance the wheel-rail adhesion.

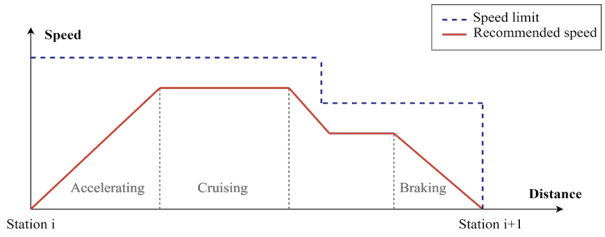

Fig. 2. Example of a train speed profile on a railway segment.

To derive appropriate observers and controllers, a model of the train system is needed. During the train operations, the vehicle travels along the track. Nevertheless, its longitudinal dynamics is nonlinear due to, for instance, its composition (locomotives and different train cars) and the couplings between the different vehicles. Furthermore, train cars do not have sensors and cannot transmit information to the ATO. Hence, existing control approaches cannot completely avoid some safety issues like coupler failure and car-derailment situations. An accurate estimation of the train car positions and the in-train forces will help with the design of improved control schemes while improving safety issues.

Furthermore, the longitudinal train dynamics is affected by other unmodeled dynamics such as the wheel-rail adhesion that varies because of tracks and weather conditions. This adhesion force is characterized by an adhesion coefficient which has a nonlinear characteristic with the wheel slip. Therefore, estimating the adhesion force and using it in the train car positions and in-train forces observer design will effectively improve the performances.

2.2 Modeling and problem statement

Let us consider a train composed of $(n-1)$ cars, with couplers between adjacent cars, and pulled by a locomotive whose longitudinal dynamics is illustrated in Figure 3.

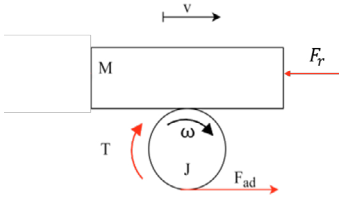

Fig. 3. Quarter-locomotive traction model.

Instead of using a simplified single-point train model, which is unpractical when many train cars and flexible couplers are considered, a multi-point train model is used to characterize the train longitudinal motion on a segment. The corresponding dynamics can be represented by the nonlinear system given as follows:

- For the locomotive (front car)

$$\begin{aligned} J_1\dot{\omega}_1(t) &= T_t(t) + T_b(t) - k\omega_1(t) - rF_{ad}(\mu) \\ \dot{x}_1(t) &= v_1(t) \\ m_1\dot{v}_1(t) &= F_{ad}(\mu) - F_{r_1}(v_1) - F_{c_1}(x_1, x_2) \\ &\quad -F_{cr_1}(x_1) - F_{d1}(x_1) \end{aligned} \tag{1}$$

- For train car i with $i = 2, ..., n-1$

$$\begin{aligned} \dot{x}_i(t) &= v_i(t) \\ m_i\dot{v}_i(t) &= F_b(t-(i-1)\tau) - F_{r_i}(v_i) \\ &\quad +F_{c_{i-1}}(x_{i-1}, x_i) - F_{c_i}(x_i, x_{i+1}) \\ &\quad -F_{cr_i}(x_i) - F_{d_i}(x_i) \end{aligned} \tag{2}$$

- For the last car n

$$\begin{aligned} \dot{x}_n(t) &= v_n(t) \\ m_n\dot{v}_n &= F_b(t-(n-1)\tau) + F_{c_{n-1}}(x_{n-1}, x_n) \\ &\quad -F_{r_n}(v_n) - F_{cr_n}(x_n) - F_{d_n}(x_n) \end{aligned} \tag{3}$$

where $\omega_1(t)$ is the locomotive wheel angular speed, m_i, $v_i(t)$ and $x_i(t)$ with $i = 1, ..., n$ represent respectively the mass, the longitudinal velocity and the position of the i^{th} car, J_1 is the inertia of the locomotive wheel, r is the wheel radius, k is the viscous friction torque coefficient and $T_t(t)$ is the locomotive traction torque, $T_b(t)$ is the braking torque, F_b is the pneumatic braking effort of the cars, τ is the time delay of the transmission of braking information from one vehicle to another. $F_{r_i}(v_i)$ is the basic resistance approximated by the Davis formula (Rochard and Schmid, 2000) as follows

$$\begin{aligned} F_{r_1}(v_1) &= a + bv_1(t) + c\sum_{i}^{n} m_i v_1^2(t) \\ F_{r_i}(v_i) &= a + bv_i(t), \qquad i = 2, \ldots, n \end{aligned} \tag{4}$$

where a, b and c are positive constants. F_{ad} is the adhesion force given by

$$F_{ad}(\mu) = \mu(\lambda)m_1 g \tag{5}$$

where g is the gravitational coefficient, and μ is an adhesion coefficient which represents the nonlinear mechanical interaction between the wheel and the rail.

Remark 1. When a wheel passes over the rail, it partially removes the contaminant from the rail. This is called the cleaning effect. Therefore, we are considering the adhesion variation on the locomotive only.

F_{c_i} is the in-train force between the i^{th} and $(i+1)^{th}$ train cars due to couplers as illustrated in Figure 4. It is approximated by a linear spring system with stiffness coefficient k_i and length l_i. Hence, the in-train force between the i^{th} and $(i+1)^{th}$ train cars can be expressed as:

$$F_{c_i}(x_i, x_{i+1}) = k_i(x_i - x_{i+1} - l_i) \tag{6}$$

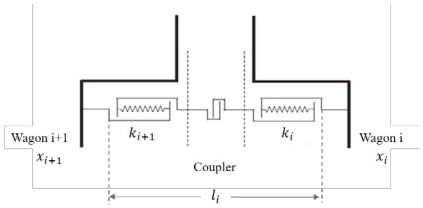

Fig. 4. Coupler model.

In this paper, it is assumed that the locomotive traction/braking force $T_t + T_b$, the pneumatic braking effort of each train car F_b and all the train parameters are perfectly known. F_{cr} is the resistive force due to track curves. It can be expressed as:

$$F_{cr_i} = m_i g \frac{k_{e_i}}{R(x_i)} \tag{7}$$

where k_{e_i} is the track gauge coefficient, and $R(x)$ is the radius of the curvature which depends on the position of the train car. F_D is the resistive force due to track declivities expressed as

$$F_{d_i} = m_i g \sin(\theta(x_i)) \tag{8}$$

where $\theta(x_i)$ is the slop angle of the track which also depends on the position of the train car.

Remark 2. The variations of the curves and slopes of the railroad are slow. For this reason, the corresponding forces are not considered in this paper.

It is assumed that the wheel angular speed of the locomotive (i.e. $\omega_1(t)$) and its position (i.e. $x_1(t)$) are measured using adequate sensors. Hence, the measurement vector is given as

$$y(t) = \begin{bmatrix} y_1(t) \\ y_2(t) \end{bmatrix} = \begin{bmatrix} \omega_1(t) \\ x_1(t) \end{bmatrix} \tag{9}$$

Note that the odometer only provides the angular wheel speed of the locomotive. This measurement cannot be used to estimate the longitudinal speed of the train due to slipping effects in the case of low adhesion between the wheel and the rail. Nevertheless, it allows to estimate the adhesion force.

The objective of this paper is to estimate the train car positions, i.e. x_i, $\forall i = 2, \ldots, n$ and the in-train forces F_{c_i} from the available measurements (9).

3. OBSERVER DESIGN FOR TRAIN CAR POSITIONS AND IN-TRAIN FORCES

3.1 Methodology

To estimate the train car positions and the in-train forces, a cascade structure of n robust sliding mode differentiators is used. The first differentiator enables to obtain in finite-time an estimate of the adhesion force, i.e. $\hat{F}_{ad}$ from the the angular wheel speed of the locomotive. Then, from

this estimate and the position of the locomotive, one can iteratively estimate the train car position, i.e. $\hat{x}_i$, $i = 2, \ldots, n$ by applying robust sliding mode differentiators. The general structure of the proposed scheme is shown in Figure 5 and Figure 6.

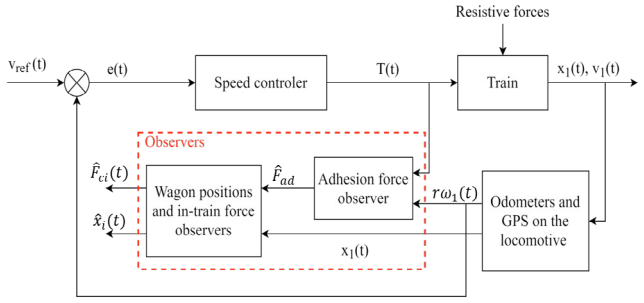

Fig. 5. Overview of the proposed estimation scheme.

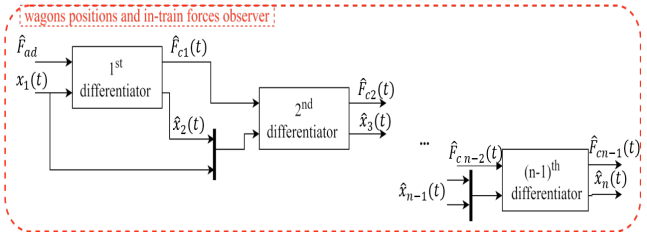

Fig. 6. Train car position and in-train forces estimation scheme.

3.2 Adhesion force observer design

Let us rewrite the wheel torque dynamic equation and the angular speed measurement as follows

$$\begin{cases} F_{ad}(\mu) &= \frac{1}{r}[T(t) - k\omega_1(t) - J_1\dot{\omega}_1(t)] \\ y_1(t) &= r\omega_1(t) \end{cases} \tag{10}$$

Here, it is assumed that ω_1 is a signal whose second derivative $\ddot{\omega}_1(t)$ is absolutely bounded by a known Lipschitz constant $L > 0$ (i.e. $|\ddot{w}_1(t)| \leq L$). To estimate the adhesion force, one must differentiate the angular velocity measurement at least once, to obtain the angular acceleration. To achieve this objective, let us apply the robust sliding mode differentiator introduced in (Levant, 2003; Levant and Livne, 2020a)

$$\begin{cases} \dot{z}_0 = -\lambda_1 L^{\frac{1}{2}}|z_0 - y_1|^{\frac{1}{2}} sign(z_0 - y_1) + z_1 \\ \dot{z}_1 = -\lambda_0 L sign(z_0 - y_1) \end{cases} \tag{11}$$

where the parameters λ_0 and λ_1 are selected as in (Levant and Livne, 2020b), i.e. $\lambda_0 = 1.1$ and $\lambda_1 = 1.5$.

The estimation error can be written as

$$e(t) = \begin{bmatrix} e_1(t) \\ e_2(t) \end{bmatrix} = \begin{bmatrix} \omega_1(t) - Z_0(t) \\ \dot{\omega}_1(t) - Z_1(t) \end{bmatrix} \tag{12}$$

From (Levant and Livne, 2020b), it is clear that the estimation error e_i, converges in a finite time t_f toward zero.

Furthermore, the estimated adhesion force is given as follows

$$\hat{F}_{ad}(\mu) = \frac{1}{r}\left[T(t) - kZ_0(t) - JZ_1(t)\right] \tag{13}$$

After the convergence time of the differentiator, one gets

$$\hat{F}_{ad} = F_{ad} \tag{14}$$

3.3 Train car positions and in-train forces observer design

From equations (1) and (6), one gets for the front car,

$$\begin{cases} F_{c_1} = F_{ad} - m_1\dot{v}_1 - a - bv_1 - cv_1^2 \sum_i^n m_i \\ x_2 = \frac{1}{k_1}(m_1\dot{v}_1 - F_{ad} + k_1(x_1 - l_1) + a + bv_1 \\ \qquad + cv_1^2 \sum_i^n m_i) \end{cases} \tag{15}$$

and for car i with $i = 2, ..., n-1$

$$\begin{cases} F_{ci} = F_b(t - (i-1)\tau) + F_{c_{i-1}} - m_i\dot{v}_i - a - bv_i \\ x_{i+1} = \frac{1}{k_i}(m_i\dot{v}_i - F_b(t - (i-1)\tau) - F_{c_{i-1}} + k_i(x_i - l_i) \\ \qquad + a + bv_i) \end{cases} \tag{16}$$

Remark 3. In practice, the coefficients (a, b, c) depend on the type and composition of the train, as well as the rail conditions. Here, it is assumed that these coefficients are known.

From (15) and using $x_1(t)$ as the output measurement, one can apply the robust second order differentiator

$$\begin{cases} \dot{Z}_{10} = -\tilde{\lambda}_{12} L^{\frac{1}{3}}|Z_{10} - y_2|^{\frac{1}{3}} sign(Z_{10} - y_2) + Z_{11} \\ \dot{Z}_{11} = -\tilde{\lambda}_{11} L^{\frac{2}{3}}|Z_{10} - y_2|^{\frac{2}{3}} sign(Z_{10} - y_2) + Z_{12} \\ \dot{Z}_{12} = -\tilde{\lambda}_{10} L sign(Z_{10} - y_2) \end{cases} \tag{17}$$

where the parameters $\tilde{\lambda}_{10}$, $\tilde{\lambda}_{20}$ and $\tilde{\lambda}_{30}$ are selected as in (Levant and Livne, 2020b), i.e. $\tilde{\lambda}_{10} = 1.1$ $\tilde{\lambda}_{11} = 2.12$ and $\tilde{\lambda}_{12} = 2$.

The estimation of the in-train force between the locomotive and the train car is given as follows

$$\begin{cases} \hat{F}_{c1} = \hat{F}_{ad} - m_1 Z_{12} - a - bZ_{11} - cZ_{11}^2 \sum_i^n m_i \\ \hat{x}_2 = \frac{1}{k_1}(m_1 Z_{12} - \hat{F}_{ad} + k_1(x_1 - l_1) + a + bZ_{11} \\ \qquad + cZ_{11}^2 \sum_i^n m_i) \end{cases} \tag{18}$$

After a finite-time, one gets

$$e_{x_2} = \hat{x}_2 - x_2 = 0 \longrightarrow \hat{x}_2 = x_2 \tag{19}$$

and

$$e_{F_{c_1}} = \hat{F}_{c_1} - F_{c_1} = 0 \longrightarrow \hat{F}_{c_1} = F_{c_1} \tag{20}$$

Furthermore, by applying the robust second order differentiator to the i^{th} car, $i = 3, \ldots, n-1$, (i.e, differentiating $\hat{x}_{i-1}$) as follows

$$\begin{cases} \dot{Z}_{(i-1)0} = -\tilde{\lambda}_{(i-1)2} L^{\frac{1}{3}}|Z_{(i-1)0} - \hat{x}_{(i-1)}|^{\frac{1}{3}} \\ \qquad sign(Z_{(i-1)0} - \hat{x}_{(i-1)}) + Z_{(i-1)1} \\ \dot{Z}_{(i-1)1} = -\tilde{\lambda}_{(i-1)1} L^{\frac{2}{3}}|Z_{(i-1)0} - \hat{x}_{(i-1)}|^{\frac{2}{3}} \\ \qquad sign(Z_{(i-1)0} - \hat{x}_{(i-1)}) + Z_{(i-1)2} \\ \dot{Z}_{(i-1)2} = -\tilde{\lambda}_{(i-1)0} L sign(Z_{(i-1)0} - \hat{x}_{(i-1)}) \end{cases} \tag{21}$$

with $\tilde{\lambda}_{(i-1)0} = 1.1$ $\tilde{\lambda}_{(i-1)1} = 2.12$ and $\tilde{\lambda}_{(i-1)2} = 2$.

The estimation of the in-train force between two adjacent train cars and its position is given as follows

$$\begin{cases} \hat{F}_{ci} = F_b(t-(i-1)\tau) + \hat{F}_{c_{i-1}} - m_i Z_{i2} - a - bZ_{i1} \\ \hat{x}_{i+1} = \dfrac{1}{k_i}[m_i Z_{i2} - F_b(t-(i-1)\tau) - \hat{F}_{c_1} + k_1(x_i - l_i) \\ \qquad + a + bZ_{i1}] \end{cases} \tag{22}$$

After a finite-time, one gets

$$e_{x_i} = \hat{x}_i - x_i = 0 \longrightarrow \hat{x}_i = x_i \tag{23}$$

and

$$e_{F_{c_i}} = \hat{F}_{c_i} - F_{c_i} = 0 \longrightarrow \hat{F}_{c_i} = F_{c_i} \tag{24}$$

Remark 4. If the measurements are affected by measurement noise, a filtering differentiator introduced in Levant and Livne (2020a) should be used to limit its impact on the estimates.

4. SIMULATION RESULTS

In this section, numerical simulations are performed to validate the effectiveness of the cascade structure of robust sliding mode differentiators introduced in Figure 5. It will be shown that the proposed robust differentiator using the angular wheel speed of the locomotive can detect low adhesion zones. It will be also shown that the proposed cascade of observers enables the finite-time estimation of the in-train forces and train cars positions.

Hereafter, two scenarios are considered.

- *scenario 1*: This scenario represents the ideal case of an undisturbed system. It shows the benefit of the proposed cascade observer
- *Scenario 2*: This scenario shows the limits of the proposed solution by considering modeling errors in terms of track slopes and curves, disturbances and measurements noise.

4.1 Simulation protocol

We simulate a train composed of a locomotive of mass of $90t$ and 10 cars, with mass of $10t$, traveling a distance of $1.4km$. Furthermore, there are three low adhesion zones at $x \in [280, 430]m$, at $x \in [590, 580]m$ and at $x \in [1200, 1350]m$ as it is shown in Figure 7. We present

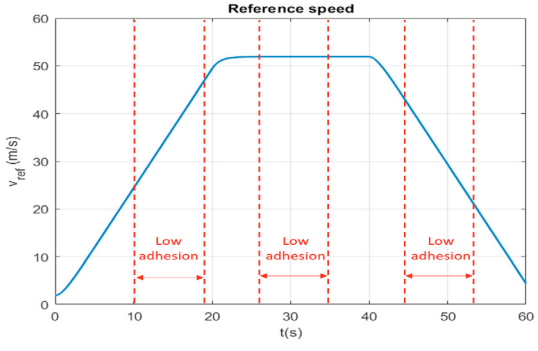

Fig. 7. Reference speed.

two scenarios: the first considers a straight flat track, and the second one, a curved sloped track. We will consider position measurement noise in the range of $[1, 5]m$ and an imperfect wheel geometry with a varying radius r in the range of $[0.53, 0.57]m$. This acts like a speed measurement noise, because speed is obtained from odometric sensors. We also consider track slope of 8 per thousand at $x = [400, 800]m$ which corresponds to $t = [17, 32]s$ and curvatures of radius of $250m$ at $x = [1200, 400]m$ which corresponds to $t = [45, 60]s$ as it is shown in Figure 8.

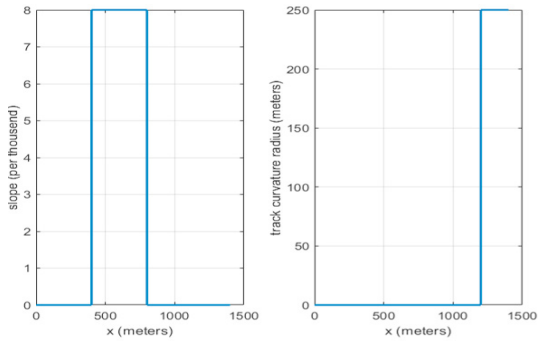

Fig. 8. Track profile.

In the following, it is assumed that the locomotive traction/braking force, the pneumatic braking effort of each train car and the drag coefficients are known. This means that the control delay is known, and the braking effort can be estimated. The train model parameters used in this simulation are given in Table 1.

Table 1. Train parameters

parameter	value
m_1	$90t$
$m_i,\ i = 2, ..., 10$	$10t$
$k_i,\ i = 1, ..., 10$	$6.5e^6\ N/m$
$l_i,\ i = 1, ..., 10$	$21\ m$
J_1	$255\ N.s^2$
r	$0.57\ m$
k	$0.01\ N.s.rad^{-1}$
a	900 N
b	$32\ N.s.m^{-1}$
c	$1\ N.s^2.m^{-1}$
τ	$0.5s$

4.2 Simulation results

The robust differentiator given in (11), (13) enables to obtain an estimate of the adhesion force with a mean estimation error of $10^{-6}N$. As shown in Figure 9, we notice peaks with a maximum amplitude of $0.1N$ at the time instants $t \in [10, 20]s$ and $t \in [45, 55]s$ corresponding to the low-adhesion zone $[280, 430]m$ and $[1200, 1350]m$ respectively. The second zone of low adhesion has no impact on the train dynamics since the traction force is null at this moment. It is shown that when the train crosses a low-adhesion zone, the adhesion force estimator is able to detect this zone in $1ms$ with an error $10mN$. There is another large peak at the time instant $20s$ with an amplitude of $0.1N$. After that, the adhesion force estimation error tends towards $10^{-6}N$ quickly with a transient time of $2s$. This is due to the change in train acceleration. We also notice oscillations around zero due to measurement noise.

In the traction phase, we notice a maximal coupler stretching of $5cm$ as it is shown in Figure 12. Note that the maximum tolerable stretching of the couplers is $23cm$. If this value is exceeded, a coupler failure will occur. We

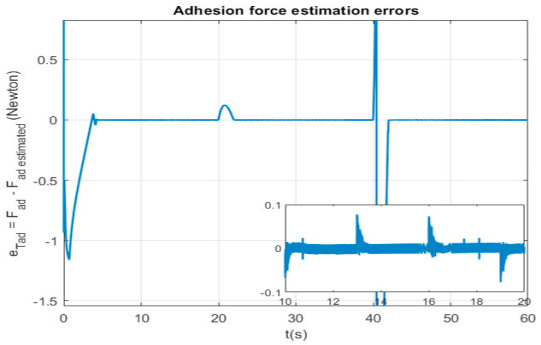

Fig. 9. Scenario 1: Adhesion force estimation error.

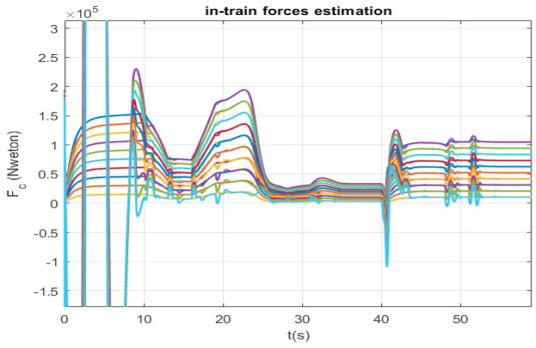

Fig. 10. Scenario 1: In-train force estimation.

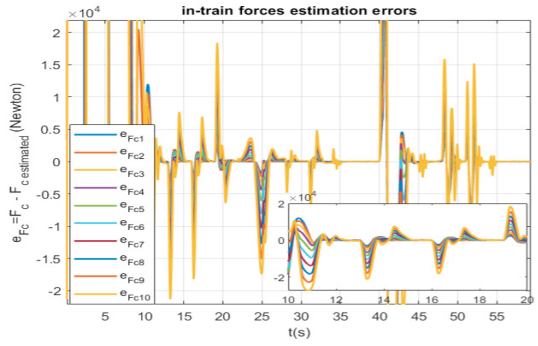

Fig. 11. Scenario 1: In-train force estimation errors.

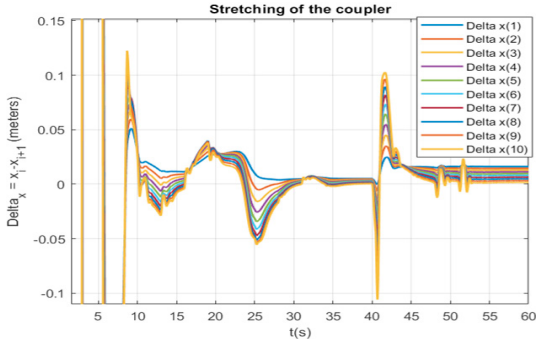

Fig. 12. Scenario 1: Couplers stretching.

also notice a peak with an amplitude of $10cm$ at $t = 40s$ which represents the transient during the variation of the acceleration. As shown in Figure 10, the couplers stretching is represented by a high in-train force effort of $150kN$ for locomotive and $15kN$ for the last wagon. When the train passes through the first low adhesion zone at time

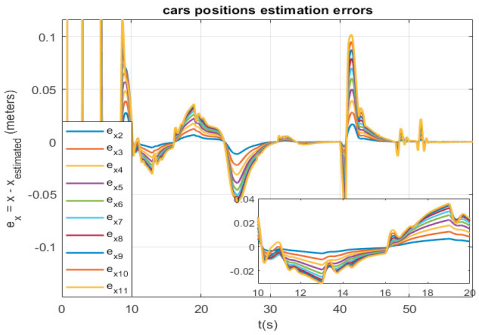

Fig. 13. Scenario 1:Cars position estimation errors.

$t = [10, 20]s$, a slip occurs, which causes a train speed reduction and thus a compression of the couplers. This phenomenon also occurs during the braking phase, when the couplings are compressed. However, when the train crosses a low-adhesion zone, the couplings are stretched. Negative peaks are also observed which correspond to the transients for each variation of acceleration or adhesion conditions.

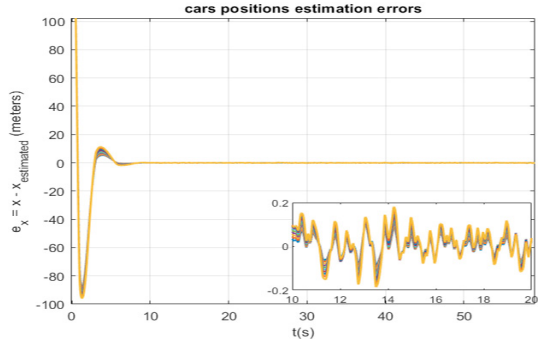

Fig. 14. Scenario 1: Estimation errors for the train car positions.

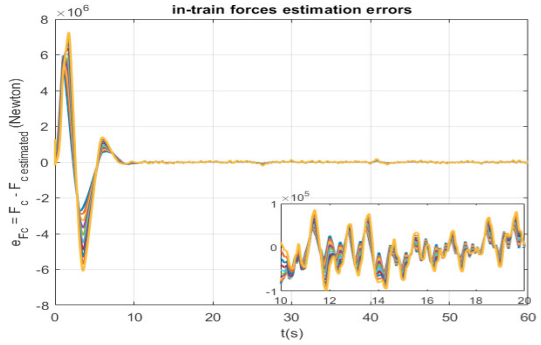

Fig. 15. Scenario 1: Estimation errors for the in-train forces.

After the transient time, the cascade of sliding mode observers for the front car (18) and the other train cars (22) accurately reconstructs the train car position with a mean estimation error of $2e^{-5}m$ as shown in Figure 14. It also enables to obtain an estimate of the in-train forces with a mean error of $1N$ as presented in Figure 15. In both figures, we notice oscillations around zero due to measurement noise which was filtered by the estimator. It is also noticed that the position measurement noise is

amplified by an average of $1cm$ after each differentiation as shown in Figure 14.

For the second scenario, we consider curves and declivities of the railway track. Figure 16 represents the estimation error of the in-train forces, and Figure 17 represents the estimation error of the car position estimation errors. A track curvature with a radius of $250m$ produces $2.65kN$ of in-train force estimation error for the first coupler and $1mm$ of car position estimation error for the first wagon, and $5.2kN$ of in-train force estimation error for the last coupler and $1cm$ of car position estimation error for the last wagon. A track slope of an angle of 8 per thousand produces $7.06kN$ in-train force estimation error for the first coupler, and $14kN$ for the last coupler, while it produces $0.4mm$ of car position estimation error for the first wagon and $4mm$ of car position estimation error for the last wagon.

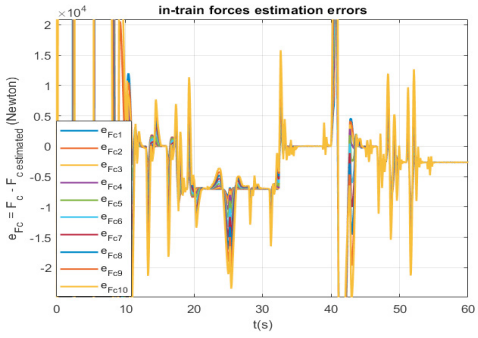

Fig. 16. Scenario 2: In-train forces estimation errors.

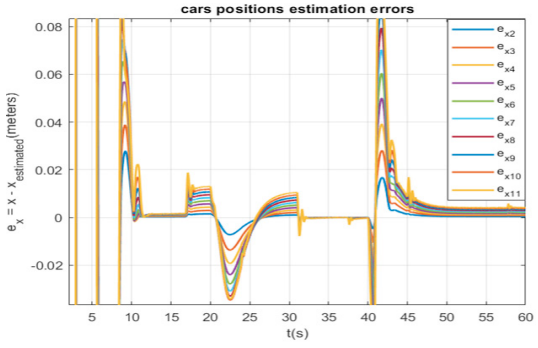

Fig. 17. Scenario 2: Cars position estimation errors.

5. CONCLUSION

This paper presents an estimation approach to reconstruct the train car positions and in-train forces, consistent with current industrial practices: locomotive-based sensors and reconstructed wheel-rail adhesion. For this purpose, a cascade structure of robust sliding mode differentiators is derived based on the multi-point train model. The first observer uses the locomotive angular speed measurement to estimate the adhesion force and to detect possible low-adhesion zones. The following $n-1$ cascade observers estimate the train car positions and in-train forces based only on the locomotive-based sensors and previous cascade estimations. Through simulation results, it is shown that the proposed scheme achieves good performances in terms of accuracy and convergence time. As a future work, we plan to use these estimates to improve train control systems design and train driving performance in avoiding train derailments and coupler failures.

ACKNOWLEDGEMENTS

This work was supported by the IRT Railenium under "Train de Fret Autonome" project.

REFERENCES

Aguiar, B., Berdjag, D., Guerra, T.M., and Demaya, B. (2018). Improving train position accuracy in case of wheel jamming faults. *IFAC-PapersOnLine*, 51(26), 25–30.

Burckhardt, M. (1993). Fahrwerktechnik: Radschlupf-regelsysteme, 1993. *Vogel-Verlag, Wurtzburg*, 36.

Chen, H., Cai, W., and Song, Y. (2014). Wheel skid prediction and antiskid control of high speed trains. In *17th International IEEE Conference on Intelligent Transportation Systems (ITSC)*, 1209–1214. IEEE.

Chen, W.H. (2004). Disturbance observer based control for nonlinear systems. *IEEE/ASME transactions on mechatronics*, 9(4), 706–710.

Chen, Y., Dong, H., Lü, J., Sun, X., and Guo, L. (2016). A super-twisting-like algorithm and its application to train operation control with optimal utilization of adhesion force. *IEEE transactions on intelligent transportation systems*, 17(11), 3035–3044.

Chou, M., Xia, X., and Kayser, C. (2007). Modelling and model validation of heavy-haul trains equipped with electronically controlled pneumatic brake systems. *Control Engineering Practice*, 15(4), 501–509.

Chou, M. and Xia, X. (2007). Optimal cruise control of heavy-haul trains equipped with electronically controlled pneumatic brake systems. *Control Engineering Practice*, 15(5), 511–519.

Cruz-Zavala, E., Moreno, J.A., and Fridman, L.M. (2011). Uniform robust exact differentiator. *IEEE Transactions on Automatic Control*, 56(11), 2727–2733.

Dabroom, A.M. and Khalil, H.K. (1999). Discrete-time implementation of high-gain observers for numerical differentiation. *International Journal of Control*, 72(17), 1523–1537.

Gao, G.j., Chen, W., Zhang, J., Dong, H.p., Zou, X., Li, J., and Guan, W.y. (2017). Analysis of longitudinal forces of coupler devices in emergency braking process for heavy haul trains. *Journal of Central South University*, 24(10), 2449–2457.

Gao, K., Huang, Z., Wang, J., Peng, J., and Liu, W. (2013). Decentralized control of heavy-haul trains with input constraints and communication delays. *Control Engineering Practice*, 21(4), 420–427.

Kalker, J. (1979). Survey of wheel—rail rolling contact theory. *Vehicle system dynamics*, 8(4), 317–358.

Kommuri, S.K., Defoort, M., Karimi, H.R., and Veluvolu, K.C. (2016). A robust observer-based sensor fault-tolerant control for pmsm in electric vehicles. *IEEE Transactions on Industrial Electronics*, 63(12), 7671–7681.

Levant, A. (2003). Higher-order sliding modes, differentiation and output-feedback control. *International journal of Control*, 76(9-10), 924–941.

Levant, A. and Livne, M. (2020a). Robust exact filtering differentiators. *European Journal of Control*, 55, 33–44.
Levant, A. and Livne, M. (2020b). Robust exact filtering differentiators. *European Journal of Control*, 55, 33–44.
Lien, C.H. (2004). Robust observer-based control of systems with state perturbations via lmi approach. *IEEE Transactions on Automatic Control*, 49(8), 1365–1370.
Liu, W.R., Wang, D.Y., Gao, K., and Huang, Z.W. (2017a). Design of distributed cooperative observer for heavy-haul train with unknown displacement. *IET Intelligent Transport Systems*, 11(4), 239–247.
Liu, X., Saat, M.R., and Barkan, C.P. (2017b). Freight-train derailment rates for railroad safety and risk analysis. *Accident Analysis & Prevention*, 98, 1–9.
Losero, R., Lauber, J., and Guerra, T.M. (2015). Transmitted torque observer applied to real time engine and clutch torque estimation. *IFAC-PapersOnLine*, 48(26), 73–78.
Pacejka, H.B. (2002). Tire and vehicle dynamics, society of automotive engineers. *Inc, Warrendale, USA*.
Pei-Xin, F. (1994). Longitudinal force of heavy haul train during traction, speed regulation and emergency brake-the testing research of 10000 t heavy haul train on da-qin railway [j]. *Journal of Southwest Jiaotong University*, 29(1), 57–64.
Rochard, B.P. and Schmid, F. (2000). A review of methods to measure and calculate train resistances. *Proceedings of the Institution of Mechanical Engineers, Part F: Journal of Rail and Rapid Transit*, 214(4), 185–199.
Tang, H.p., Tang, Y.j., and Tao, G.a. (2006). Active vibration control of multibody system with quick startup and brake based on active damping. *Journal of Central South University of Technology*, 13(4), 417–421.
Uyulan, Ç. and Gokasan, M. (2018). Modeling, simulation and re-adhesion control of an induction motor–based railway electric traction system. *Proceedings of the Institution of Mechanical Engineers, Part I: Journal of Systems and Control Engineering*, 232(1), 3–11.
Wang, S. and Xia, X. (2003). Mathematical modelling of heavy-ore load train equipped with electronically control pneumatic brake.
Wang, Z. and Jia, Y. (2018). A terminal sliding mode algorithm for train velocity tracking considering wheel-rail adhesion. In *2018 Chinese Automation Congress (CAC)*, 3065–3069. IEEE.
Xia, X. and Zhang, J. (2011). Modeling and control of heavy-haul trains [applications of control]. *IEEE Control Systems Magazine*, 31(4), 18–31.
Yang, L., Luo, S., Fu, M., et al. (2014). Study on effect of longitudinal impulse for 20,000 t heavy combined train. *Electr Drive Locomot*, 3, 34–39.
Zhang, L. and Zhuan, X. (2014). Development of an optimal operation approach in the mpc framework for heavy-haul trains. *IEEE Transactions on Intelligent Transportation Systems*, 16(3), 1391–1400.
Zhu, B. and Xia, X. (2015). Nonlinear trajectory tracking control for heavy-haul trains. *IFAC-PapersOnLine*, 48(11), 41–46.